

Article

# Differential Evolution Based Algorithm for Optimal Current Ripple Cancelation in an Unequal Interleaved Power Converter

Julio C. Rosas-Caro <sup>1,\*</sup>, Pedro M. García-Vite <sup>2</sup>, Alma Rodríguez <sup>1,3</sup>, Abraham Mendoza <sup>1</sup>,  
Avelina Alejo-Reyes <sup>1</sup>, Erik Cuevas <sup>3</sup> and Francisco Beltran-Carbajal <sup>4</sup>

<sup>1</sup> Facultad de Ingeniería, Universidad Panamericana, Alvaro del Portillo 49, Zapopan 45010, Mexico; anrodriguez@up.edu.mx or alma.rvazquez@academicos.udg.mx (A.R.); amendoza@up.edu.mx (A.M.); aalejo@up.edu.mx (A.A.-R.)

<sup>2</sup> Tecnológico Nacional de México, Instituto Tecnológico de Ciudad Madero, Av. 1o. de Mayo s/n Col. Los Mangos, Ciudad Madero 89440, Mexico; pedro.gv@cdmadero.tecnm.mx

<sup>3</sup> Departamento de Electrónica, Universidad de Guadalajara, CUCEI, Av. Revolución 1500, Guadalajara 44430, Mexico; erik.cuevas@cucei.udg.mx

<sup>4</sup> Departamento de Energía, Universidad Autónoma Metropolitana, Unidad Azcapotzalco, Mexico City 02200, Mexico; fbeltran@azc.uam.mx

\* Correspondence: crosas@up.edu.mx; Tel.: +52-33-1918-1065

**Abstract:** This paper proposes an optimal methodology based on the Differential Evolution algorithm for obtaining the set of duty cycles of a recently proposed power electronics converter with input current ripple cancelation capability. The converter under study was recently introduced to the state-of-the-art as the interleaved connection of two unequal converters to achieve low input current ripple. A latter contribution proposed a so-called proportional strategy. The strategy can be described as the equations to relate the duty cycles of the unequal power stages. This article proposes a third switching strategy that provides a lower input current ripple than the proportional strategy. This is made by considering duty cycles independently of each other instead of proportionally. The proposed method uses the Differential Evolution algorithm to determine the optimal switching pattern that allows high quality at the input current side, given the reactive components, the switching frequency, and power levels. The mathematical model of the converter is analyzed, and thus, the decision variables and the optimization problem are well set. The proposed methodology is validated through numerical experimentation, which shows that the proposed method achieves lower input current ripples than the proportional strategy.

**Keywords:** Differential Evolution; metaheuristic algorithms; optimization; DC–DC converter



**Citation:** Rosas-Caro, J.C.; García-Vite, P.M.; Rodríguez, A.; Mendoza, A.; Alejo-Reyes, A.; Cuevas, E.; Beltran-Carbajal, F. Differential Evolution Based Algorithm for Optimal Current Ripple Cancelation in an Unequal Interleaved Power Converter. *Mathematics* **2021**, *9*, 2755. <https://doi.org/10.3390/math9212755>

Academic Editor: Nicu Bizon

Received: 28 September 2021

Accepted: 21 October 2021

Published: 29 October 2021

**Publisher's Note:** MDPI stays neutral with regard to jurisdictional claims in published maps and institutional affiliations.



**Copyright:** © 2021 by the authors. Licensee MDPI, Basel, Switzerland. This article is an open access article distributed under the terms and conditions of the Creative Commons Attribution (CC BY) license (<https://creativecommons.org/licenses/by/4.0/>).

## 1. Introduction

Power electronics converters are essential in many fields of applications. Particularly, DC–DC power converters range from a few watts in battery-powered portable devices [1–3] to several kilowatts when employed in power systems [4,5]. Portable electronics devices usually operate at high frequencies in order to reduce their physical sizes [2]. This research focuses on a DC–DC step-up power converter. This kind of converter can be employed in renewable energy sources with low D.C. power generation, such as photovoltaic and hydrogen-based fuel cell sources that provide a few tens of volts [6]. DC–DC converters are constituted by a combination of solid-state switches and reactive components that process the input power to feed a resistive load, usually at different voltage levels. The switches are driven by a binary commanding function  $q(t)$  at a fixed frequency. The reactive components capacitors ( $C$ ) and inductors ( $L$ ) are employed to store the energy coming from the source and then deliver such energy to the load.

Among the features specified in a high voltage-gain DC–DC converter is the voltage gain; this can be defined as the output voltage ratio to the input voltage and is independent

of the reactive components. Another important specification is the input current quality, which is analyzed in terms of the switching ripple. This is the article's main focus, and it is related to current drawn from the source; having a high input current quality means that a pure (or almost pure) D.C. is extracted, without A.C. ripple or variation. This is an ideal condition since the ripple naturally appears due to the commutation process of the switches. Several topologies that provide high input current quality have recently appeared in the literature [7–10]. With the modification of a conventional boost converter presented in [11], it is possible to have a reduced input current ripple by adding extra components. More complex configurations with both capabilities have also been proposed.

This paper focuses on a recently proposed converter [12], made by the interleaved connection of two unequal power stages, the classical boost converter [13] and a modified (resonant version of the) three-switch high-voltage TSHV converter [14].

The interleaved interconnection of classical boost power stages is a proven technology [15]. It leads to a special situation in which the input current ripple is zero (for  $D = 0.5$ ); in this zero-ripple situation, the input current ripple (high-frequency variation) of one power stage cancels perfectly with the other one (for example, in a two-phases converter), and the input current of the entire converter is a pure D.C. signal. However, this happens only in a particular operation point; for different duty cycles ( $D \neq 0.5$ ), the ripple must be evaluated.

The contribution made in [12] was not only the interconnection of two unequal power stages. The interconnection, along with a particular PWM strategy (in which duty cycles of power stages were opposite or complementary), made it possible to choose the zero-ripple point or zero ripple duty cycle (it can be  $D = 0.5$  or any other). Another contribution related to this converter was reported in [16], in which a different PWM strategy, and design procedure, were introduced. In ref. [16], the duty cycles of power stages are proportional instead of complementary to each other, allowing a better operation of the converter and reducing the input current ripple of the entire converter.

This article proposes a third PWM strategy for the discussed converter. In this case, duty cycles of the unequal power stages are independent of each other, and this makes it possible to further reduce the input current ripple of the entire operating range of the converter without changing the hardware (physical components) of the circuit. Having independent duty cycles brings a particular challenge; an infinite number of combinations of duty cycles provide a specific voltage gain. This challenge is solved by using the Differential Evolution DE algorithm. The DE algorithm is used to select the combination of duty cycles that comply with the required output voltage, and at the same time, minimizes the input current ripple of the converter. The proposed methodology is validated through numerical experimentation, which shows that the proposed method achieves a better result (lower input current ripple) than the proportional strategy for a predefined operation range.

Optimization algorithms are widely used in the electrical engineering field [17–22]. Other related approaches that use metaheuristic algorithms, particularly for DC–DC converters, have been recently proposed. These methods include the Harris Hawks Optimization (HHO) algorithm, which is applied for tuning the parameters of two PID controllers used in a buck converter by minimizing the maximum overshoot [18]. In addition, a hybrid method was proposed in [19] that uses the Firefly (F.A.) and Particle Swarm Optimization (PSO) algorithms to adjust the parameters of the PID controller used in a buck converter. Furthermore, the same problem of tuning parameters of the PID controller in a DC–DC buck converter was managed by a hybrid strategy that integrated the Whale Optimization Algorithm and Simulated Annealing to enhance the transient response of the converter [20]. Similar approaches were proposed in [21,22] to face the parameter tuning problem in the PID controllers of converters of this type.

## 2. Converter Configuration

The interconnection of two or more power stages or cells is a common practice to build more complex converters, and the proposition of new topologies is a very active

research field. There are many composed topologies; for example, the interleaved boost converter [15]. Despite the large number of different combinations, a large portion belongs to two main configurations. Considering two individual power cells (Cell 1 and Cell 2) with the voltage gain represented by the functions  $g_1(d_1)$  and  $g_2(d_2)$ , respectively, two possible configurations can be obtained (see Figure 1). The first configuration shown in Figure 1a is the cascaded interconnection; the output of the first power stage is the input of the second one. The second configuration is the input-parallel output-series, in which power stages are connected in parallel at the input, and in series at the output.

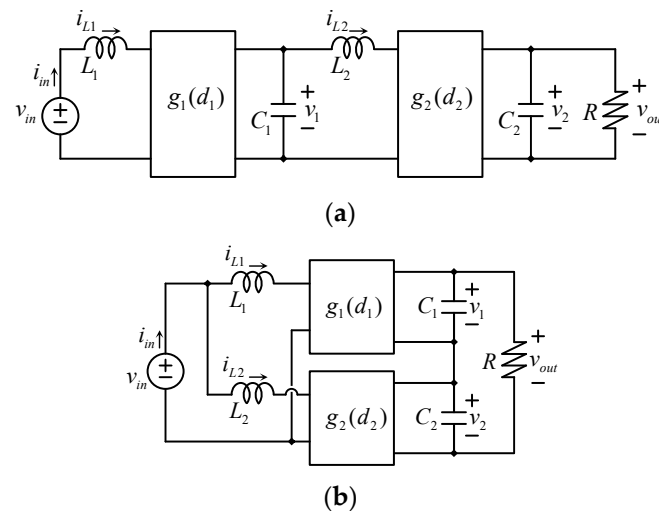


**Figure 1.** Two common configurations of two power cells to obtain high voltage gain: (a) cascaded configuration; (b) input-parallel output-series configuration.

The independent variables  $d_1$  and  $d_2$  are the duty cycles corresponding to each converter. Figure 1a shows a cascaded connection where the output voltage  $v_o$  is the input voltage times the product of the individual gains. In contrast, in Figure 1b, the value of  $v_o$  is the voltage times the summation of the individual gains of each power stage. The common feature of both configurations is that the source current is diverted into the two cells through its corresponding input inductor. Good examples of both configurations can be found in [16] for a photovoltaic application and in [23] adapted for DC-source renewable generation.

In the second case, the input-parallel output-series configuration, it is true that:

$$i_{in}(t) = i_{L1}(t) + i_{L2}(t) \quad (1)$$

The proposed methodology is applied to a power converter belonging to the input-parallel output-series configuration [12,22].

### 3. Converter Understudy

In order to apply the proposed methodology, the mathematical model of the selected power converter is first derived. Figure 2 shows the converter understudy, initially proposed in [12]. The converter is composed of two cells in an input-parallel output-series connection, following the configuration presented in Figure 1b.

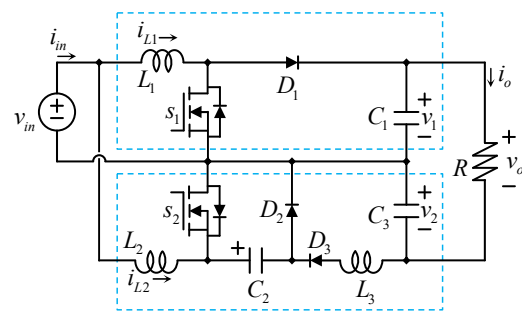


Figure 2. Configuration of the converter under study.

The cells that build the selected converter are: (i) A boost converter [13] composed of switch  $S_1$ , diode  $D_1$ , inductor  $L_1$ , and capacitor  $C_1$ . (ii) A modified (resonant version of the) three-switch high-voltage TSHV [14] converter constituted by the rest of the devices, that is, switch  $S_2$ , diode  $D_2$ , inductors  $L_2$  and  $L_3$ , and capacitors  $C_2$  and  $C_3$ ; note that diode  $D_3$  has been added to block negative current through  $L_3$ .

The load resistor  $R$  is fed by the summation of the individual output voltage of each cell, that is,  $v_{C1}$  for the boost converter and  $v_{C3}$  for the modified TSHV converter; therefore, the instantaneous output voltage  $v_o(t)$  is determined by (2).

$$v_o(t) = v_{C1}(t) + v_{C3}(t) \tag{2}$$

It is worth mentioning that there are other hybrid topologies, such as [24], but the structure of Figure 2, driven by two independent transistors, makes it possible to perform the input current ripple cancelation, as will be explained.

### 3.1. Mathematical Model of the Power Converter

Transistors are the manipulated devices that allow power processing through the reactive components. Therefore, in the selected topology, two switching functions are independently operated, which are defined as (3).

$$q_j(t) = \begin{cases} 1 & \rightarrow S_j \text{ is closed} \\ 0 & \rightarrow S_j \text{ is open} \end{cases} \tag{3}$$

with  $j = 1, 2$  corresponding to switches  $S_1$  and  $S_2$ . Since there are two switching functions that are independently controlled, four possible combinations are obtained.

For practical realization, the switching functions of (3) can be implemented in digital or analog fashion in the well-known pulse-width modulation (PWM) technique, which consists of commutating the transistor at constant frequency  $F_S$ , and hence, at constant period  $T_S = 1/F_S$ . Assuming that  $q_j(0) = 1$ , the transition occurs at  $t = dT_S$ , as illustrated in Figure 3.

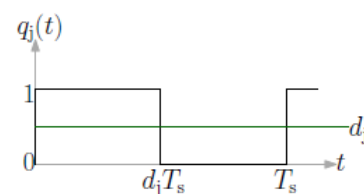


Figure 3. Graphical representation of the switching functions  $q_j(t)$  as a PWM technique.

The ratio of the time during which the transistor is active (on-state) to the time when it is inactive (off-state) is called the duty cycle  $d_j(t)$  and is equivalent to the average value of the switching function, as (4) indicates.

$$d_j(t) = \frac{1}{T_S} \int_t^{t+T_S} q_j(\tau) d\tau \tag{4}$$

Note that  $d_j(t)$  is usually taken as a function of time. It represents the manipulated variable that can vary from one switching period to another during the transient response when a closed-loop is implemented [25].

### 3.2. Equivalent Circuits

In the converter understudy, the input current depends on the inductor’s current, and the action of the switching functions drives the inductor’s current.

The best case to minimize the input current (see Figure 4) is when transistors switch complementarily, which means when  $S_1$  is open,  $S_2$  is closed, and vice versa. This strategy was originally proposed in [12] and consisted of commutating between the equivalent circuits of Figure 4a,b. All switching states are summarized in Table 1.

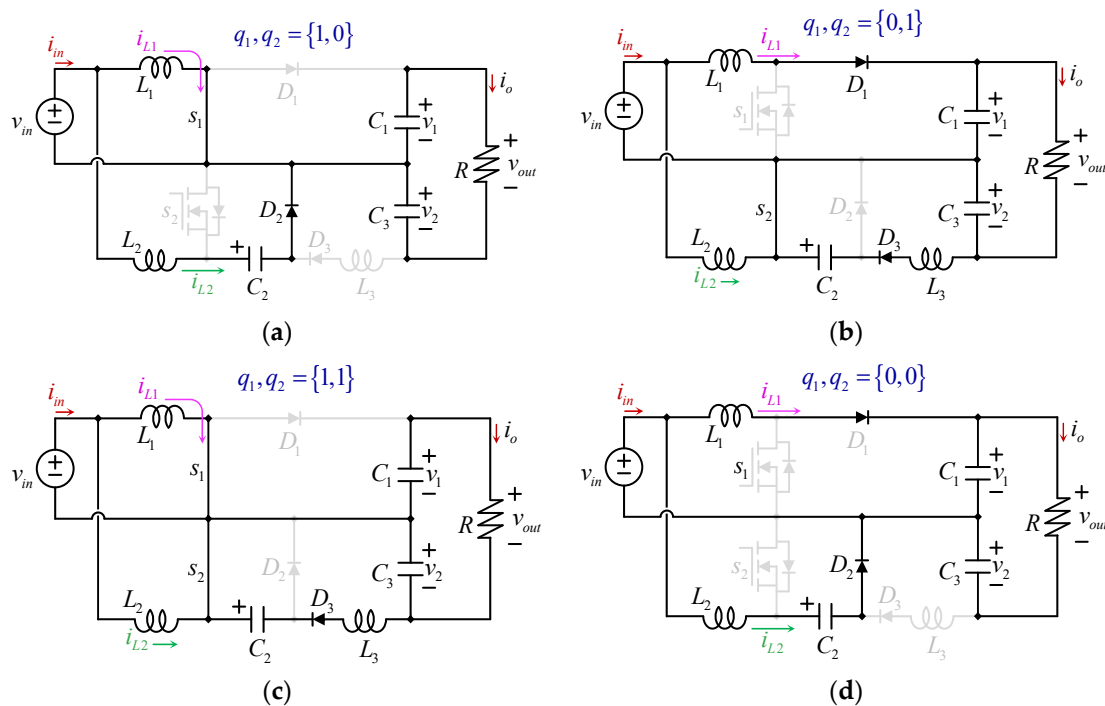


**Figure 4.** Equivalent circuits for the various commutation states: (a) state:  $q_1, q_2 = \{1,0\}$ , current through  $L_1$  increases whereas that which runs through  $L_2$  decreases; (b) state:  $q_1, q_2 = \{0,1\}$ , opposite to the state in (a); (c) state:  $q_1, q_2 = \{1,1\}$ , both inductors’ currents increase; and (d) state:  $q_1, q_2 = \{0,0\}$ , both inductors’ currents decrease.

**Table 1.** State.

S <sub>1</sub>	S <sub>2</sub>	Circuit
0	0	a
0	1	b
1	0	c
1	1	d

### Average Model of the Converter

The instantaneous voltage  $v_x(t)$  across an inductor  $L_x$  is defined as:

$$v_x(t) = L_x \frac{di_x(t)}{dt} \quad (5)$$

Since, in power electronics converters, the voltage across an inductor during a commutation state, as well as the inductance, is constant, it can be observed that the derivative is constant, and the current changes (rises or falls) linearly. For a positive voltage of  $v_x(t)$ , the current  $i_x$  increases with a constant slope, whereas the current decreases with a constant slope for negative values of  $v_x(t)$ . This consideration is usually called small ripple approximation or linear ripple approximation [13], and it is justified considering that passive components are correctly chosen for this purpose.

Therefore, due to the commutation action, the inductor currents possess a triangular-shaped waveform.

From the circuits of Figure 4a,b and following the average model theory, it is possible to write the inductor voltage along the entire switching period, as in (6) and (7).

$$\frac{di_{L1}}{dt} = d_1 \frac{v_{in}}{L_1} + (1 - d_1) \frac{v_{in} - v_{C1}}{L_1} \quad (6)$$

$$\frac{di_{L2}}{dt} = d_2 \frac{v_{in}}{L_2} + (1 - d_2) \frac{v_{in} - v_{C2}}{L_2} \quad (7)$$

The steady state can be calculated by considering that if the derivatives in (6) and (7) are zero, the capacitors' voltages are found to be:

$$V_{C1} = \frac{v_{in}}{(1 - D_1)} \quad (8)$$

$$V_{C2} = \frac{v_{in}}{(1 - D_2)} \quad (9)$$

It is worth noting that the variables are capitalized in order to denote the average values of the steady state or equilibrium.

## 4. Existing Methods

This article proposes a modulation strategy for a converter for which two modulation strategies have been used; we can call them (i) the complementary strategy, proposed in [12], and (ii) the proportional strategy, proposed in [16].

### 4.1. The Complementary Strategy

The complementary strategy, proposed in [12], consists of defining the duty cycles, as shown in (10) and (11).

$$D_1 = (1 - D) \quad (10)$$

$$D_2 = D \quad (11)$$

Important waveforms related to the complementary strategy can be appreciated in Figure 5.

Taking (2), (8), and (9) into account, the voltage gain ( $G_{comp} = V_o / V_{in}$ ) for the complementary strategy can be calculated as (12).

$$G_{comp} = \frac{1}{D(1 - D)} \quad (12)$$

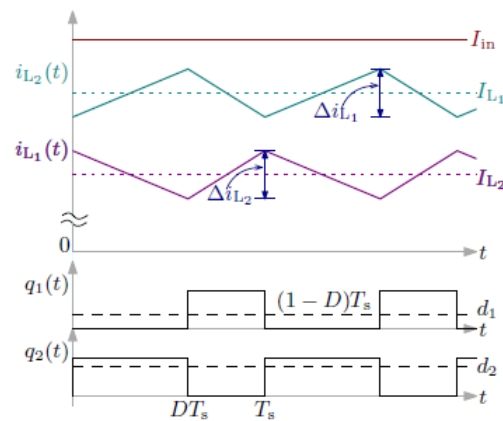


Figure 5. Graphical representation of the switching functions  $q_j(t)$ : complementary PWM technique.

For the proposed strategy presented in [12], it is easy to find the average current through inductors, as shown in (13) and (14):

$$I_{L1} = \frac{1}{D} I_o \tag{13}$$

$$I_{L2} = \frac{1}{(1 - D)} I_o \tag{14}$$

where the output current  $I_o = V_o/R$ . Moreover, from the equivalent circuits for  $q_1, q_2 = \{1,0\}$  and  $q_1, q_2 = \{0,1\}$ , the current ripples in each inductor can be readily quantified, as shown in (15) and (16).

$$\Delta i_{L1} = \frac{V_{in}}{L_1} \frac{(1 - D)}{F_s} \tag{15}$$

$$\Delta i_{L2} = \frac{V_{in}}{L_2} \frac{D}{F_s} \tag{16}$$

Following (1), the input current ripple can be expressed as shown (17) and (18).

$$\Delta i_{in} = \Delta i_{L1} + \Delta i_{L2} \tag{17}$$

However, the inductor current ripples have a phase displacement of  $180^\circ$  (see Figure 5); in other words, they always have different signs, for which the input current ripple can be expressed as the difference among (15) and (16), and not their summation. Therefore, the input current ripple is defined as:

$$\Delta i_{in} = \left| \frac{V_{in}}{F_s} \left( \frac{D}{L_2} - \frac{1 - D}{L_1} \right) \right| \tag{18}$$

From (18), it is easy to solve for D to obtain a zero-current ripple at the converter’s input.

This strategy can fully cancel the current ripple at a preestablished operating point. However, as the converter moves away from such a point, the input current increases undesirably.

#### 4.2. Proportional Modulation Strategy

The strategy described above is able to draw a D.C. pure current from the power source. The proportional strategy, proposed in [16], also makes it possible to perform the zero-ripple operation for a particular operation point, but converters usually operate not only on a specific operation point but into an operating range. It was shown in [16] that both strategies provide the same performance in the zero ripple operation points. Still, in different operation points, the proportional strategy provided a smaller input current ripple. That means, for a predefined operation range, the proportional strategy performs better.

Considering (2), (8), and (9) the voltage gain  $G$  can be expressed as (19) and (20) for duty cycles  $D_1$  and  $D_2$ .

$$G = \frac{1}{(1 - D_1)} + \frac{1}{(1 - D_2)} \tag{19}$$

$$G = \frac{2 - D_1 - D_2}{1 - D_1 - D_2 + D_1 D_2} \tag{20}$$

Equations (19) and (20) apply for the converter in all different strategies.

It is evident that the desired voltage gain  $G_1$  can be obtained with an infinite number of combinations of duty cycles employed in (19) and (20). The strategy proposed in [16] assigns a proportional relationship, as shown in (21) and (22).

$$D_1 = kD \tag{21}$$

$$D_2 = D \tag{22}$$

where the factor  $k$  is a constant value, determined during the design process as a function of the inductors in the following manner:

$$k = \frac{L_1}{L_2} \tag{23}$$

Considering (20)–(22), the voltage gain can be expressed as (24).

$$G_k = \frac{2 - D - kD}{1 - D + D + kD^2} \tag{24}$$

As it was presented in [16], the input current ripple can be analyzed in two different cases; let's consider  $d^*$  as the duty cycle in which the input current ripple is zero (as in [16]). The input current ripple is expressed differently when  $d < d^*$  and when  $d > d^*$ . Figure 6 shows important waveforms of the operation: (i) in the case for  $d < d^*$ , and (ii) in the case for  $d > d^*$ . Figure 6 shows the graphical representation of both cases.

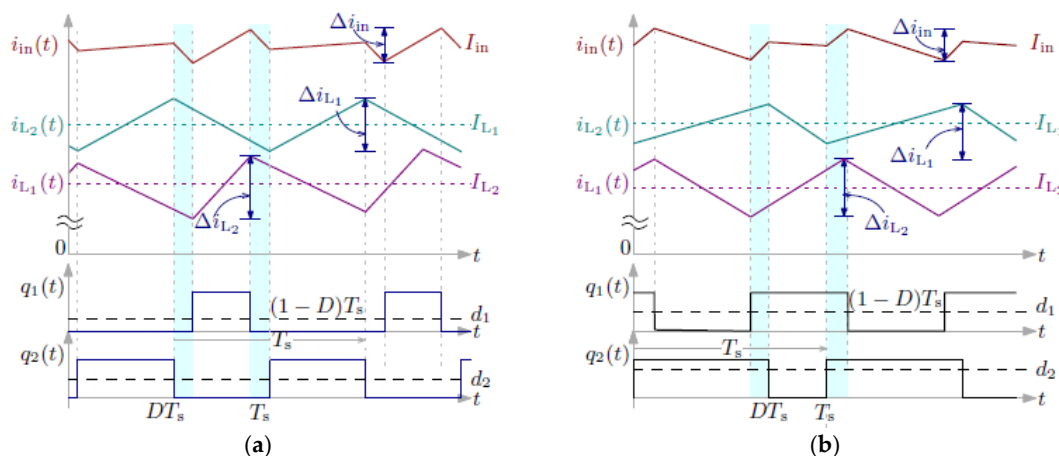


Figure 6. (a)  $D_1 = 30\%$ ,  $D_2 = 50\%$ ; (b)  $D_1 = 30\%$ ,  $D_2 = 70\%$ .

Although the input current ripple behaves slightly differently in both cases, the input current ripple can be defined as the maximum ripple during the operation. Then, the largest value is provided by the calculation in both cases [16].

It is worth mentioning that a PID controller still may control the voltage gain of the converter to achieve the desired output voltage. The discussed algorithms are designed to decide the proportions of duty cycles or of voltage gain in individual power stages of the composing converter. The design of the PID controller can still be based on an optimization algorithm [18–21].

## 5. Differential Evolution Algorithm

Differential Evolution (D.E.) [26–31] is a search method that is widely recognized in the evolutionary community and has proven its effectiveness and robustness in finding global solutions. The DE algorithm is a classic and popular method that is extensively used to solve complex optimization problems. Its low complexity and high performance have made it widely used for applications in different fields such as image processing, operation research, electronics engineering, mechanical engineering, manufacturing design, power engineering, and many others [30,31]. Although other sophisticated evolutionary methods have been recently proposed, the D.E. algorithm still maintains its prestige in the metaheuristic community, mainly because of its low computational cost and effectiveness even in constrained and high-dimensional optimization problems [29].

The DE technique considers different operators in its search strategy that allow the particles to improve as they evolve in each generation. The DE method process involves three basic operators, which are mutation, crossover, and selection. These operators are part of the algorithm search process and will be described in detail in this section.

### 5.1. Mutation

The mutation process generates a mutant vector that results from combining the information from three different vectors,  $x_{r1}$ ,  $x_{r2}$ , and  $x_{r3}$ , taken randomly from the population. The combination of these vectors considers the scaled difference between two of the three vectors. Then, this difference is added to the third vector. The mathematical representation of the mutation operator is described as:

$$v = x_{r3} + F(x_{r1} - x_{r2}) \quad (25)$$

Each vector represents an individual from the population given in the presented equation, while every element of the vector represents one dimension of the optimization problem. The scale factor  $F$  from the same equation controls the difference between the vector  $x_{r2}$  and the vector  $x_{r3}$ . According to the authors of the D.E. algorithm, the scale factor can take values within the interval  $[0, 2]$ . The scale factor is also known as the differential weight since it regulates the difference  $(x_{r1} - x_{r2})$ .

### 5.2. Crossover

The crossover operator combines the information from one individual with the information from the mutant vector. This mechanism gives diversity to the population and, therefore, prevents the algorithm from stagnating in suboptimal solutions. The combination consists of randomly taking elements from the mutant vector and elements from one individual from the population with the aim of building a test vector  $u$ . The crossover operation includes a crossover probability  $P_{cross}$  that adjusts the contribution of the mutant vector in the generation of the test vector. The crossover probability strongly influences the effectiveness of the D.E. method in finding promising solutions. Therefore, it is considered a parameter to be adjusted by selecting values within the interval  $[0, 1]$ . The crossover operator definition is expressed as (26).

$$u_j = \begin{cases} v_{ij} & r(0,1) \leq P_{cross} \\ x_{ij} & otherwise \end{cases} \quad (26)$$

### 5.3. Selection

The selection operator is the last stage in the D.E. method's flow of operations. The objective of the selection method is to determine whether an individual in the population is replaced by the test vector generated with the mutation and crossover operators. The replacement of the individual with the test vector is carried out based on the evaluation of the quality of both solutions. The individual who is selected through this evaluation process

becomes part of a new generation of individuals. In this way, this mechanism ensures that individuals evolve by selecting only the best particles to be part of a new population.

The selection mechanism contemplates the fitness value of the test vector  $u$  and the fitness value of the individual  $x_i$ . The selection follows a simple rule; if the fitness value of the individual is worse than the fitness value of the test vector, then the individual is replaced by the test vector. Otherwise, no replacement is made. Thus, the selection can be formulated as:

$$x_i = \begin{cases} u, & f(u) \leq f(x_i) \\ x_i, & otherwise \end{cases} \tag{27}$$

### 6. The Proposed Strategy

The proposed strategy considers two independent duty cycles, in contrast to the former two strategies, namely the complementary strategy [12] defined in (10) and (11), and the proportional strategy [16] defined by (21) and (22). Equations (2), (8), and (9) still define the output voltage, which can also be expressed as (19) and (20). However, in this case, there is not a particular equation that relates both duty cycles.

The strategy can be defined as (28) and (29).

$$D_1 = k_d D \tag{28}$$

$$D_2 = D \tag{29}$$

where the factor  $k_d$  is not a constant value, as in (21) and (22), but is instead a variable that has to be found at the same time as  $D_1$  and  $D_2$ .

The problem can be defined as an optimization problem. The objective is to minimize the input current ripple while, at the same time, finding the duty cycles  $D_1$  and  $D_2$ . Finding  $D_1$  and  $D_2$  is equivalent to finding  $D$  and  $k_d$  (see (28) and (29)). An important restriction of the problem is the need to comply with a required amount of voltage gain. The input current ripple can be defined as the largest of Equations (30) and (31).

$$\Delta i_{g1} = \frac{V_{in}}{k_L f s L_2} (k_L - k_d D - k_L k_d D) \tag{30}$$

$$\Delta i_{g2} = \frac{V_{in}}{k_L f s L_2} (1 - D - k_L D) \tag{31}$$

where  $k_L$  represents the relations among inductors (same as (23) for [16]), which must be provided to the optimization problem.

An optimizer is ideal for this problem since the input current ripple is variable, and their minimum value depends on the operating condition. The optimizer can minimize the input current ripple without the need for a particular desired value (or setpoint) for the ripple.

#### 6.1. The Objective Function

The optimization problem is formulated according to the objective function defined in (32). This objective function minimizes the higher value of the input current ripple. This means that it evaluates Equations (30) and (31) and considers the highest value of the two current ripple calculations to change parameters  $D$  and  $k_d$  in order to decrease this value.

$$\min_{D, k_d \in \mathbb{R}} f(D, k_d) = \begin{cases} \Delta i_{g1}, & \Delta i_{g1} > \Delta i_{g2} \\ \Delta i_{g2}, & otherwise \end{cases} \tag{32}$$

The above equation is subject to:

$$\frac{V_{out}}{V_g} \leq \frac{2 - D - k_d D}{(1 - k_d D)(1 - D)} \leq \frac{V_{out}}{V_g} + \delta \tag{33}$$

$$0 \leq D \leq 1 \tag{34}$$

$$0 \leq k_d \leq 1 \tag{35}$$

The objective function is subject to some constraints given by Equations (33)–(35). Equations (34) and (35) define the range of possible values that parameters  $D$  and  $k_d$  can adopt. On the other hand, Equation (33) restricts the value of the output voltage. It ensures that the desired voltage gain is satisfied. Equation (33) also contemplates a tolerance in the output voltage, which is 1% of the estimated voltage gain. The solution obtained by the proposed method must accomplish three such restrictions in order to consider the solution as a feasible one.

### 6.2. Computational Procedure

The proposed strategy considers the implementation of the Differential Evolution algorithm to find the optimal values of the parameters  $D$  and  $k_d$ , which control the duty cycle of the hybrid switched-capacitor boost converter. Currently, the optimal operation of this type of converter is given by a specific duty cycle, which is obtained from a dependent relationship between parameters  $D$  and  $k_d$ . The dependency between these parameters limits a further reduction in the input current ripple. Therefore, this article proposes a different strategy to find the optimal switching pattern that allows high quality at the input current side, thereby providing the reactive components with the required switching frequency and power levels.

The optimization algorithm considers the set of values  $D$  and  $k_d$  as a possible solution. Thus, a population of possible solutions is created so that every individual  $i$  from the population is defined as (36).

$$x_i = \{D, k_d\} \tag{36}$$

The population size is determined by the parameter  $N$ , which must be set at the beginning of the search process. Additionally, every individual from the population is initialized, by assigned random values, to the set  $\{D, k_d\}$ . Then, each individual’s fitness value is calculated employing the objective function, which determines the input current ripple. The assigned values to the set  $\{D, k_d\}$  must satisfy the required gain both in the initialization phase and throughout the algorithm search process. Therefore, the objective function includes a constraint that identifies the particles that do not meet this requirement. The identified solutions that violate this constraint are penalized by increasing their fitness values. This mechanism avoids unfeasible solutions, and, at the same time, it guides the search towards the space of feasible solutions. In that sense, to include the penalization, the fitness function is rewritten as (37).

$$fitness = \min_{x_i \in \mathbb{R}^2} f(x_i) + h \tag{37}$$

From the above equation, the penalty function “ $h$ ” is responsible for increasing the fitness value of the particles that have violated the restriction. The mathematical expression of this function is given by (38).

$$h = aC \left| \frac{V_{out}}{V_g} - \frac{2x_{i1} - x_{i2}x_{i1}}{(1 - x_{i1}x_{i2})(1 - x_{i1})} \right| \tag{38}$$

Here,  $a$  is a constant factor that controls the penalization degree of every unfeasible solution. Whenever there is an unfeasible solution, the activation function  $C$  sets its value to one to perform the penalty function. Otherwise, the penalty function is switched off. The definition of the activation function can be expressed as (39).

$$C = \begin{cases} 0, & \frac{2-x_{i1}-x_{i2}x_{i1}}{(1-x_{i2}x_{i1})(1-x_{i1})} \geq \frac{V_{out}}{V_g} \\ 1, & otherwise \end{cases} \tag{39}$$

The general structure of the D.E. method consists of initializing the population and evaluating its fitness value. Then, the mutation operation is performed for each particle to generate its mutant vector. After that, the crossover operation is also applied to every candidate solution to create its test vector. Finally, the test vectors are evaluated in terms of the fitness function. The best fitness between every particle and its respective test vector is considered as the selection criterion to determine the set of individuals that will remain for the next generation. This routine continues repeating for a specific number of generations, denoted as  $G_{max}$ . After all, the best solution found up to this point will represent the values of parameters  $D$  and  $k_d$ . The described procedure is summarized in Algorithm 1.

---

**Algorithm 1** The general structure of the D.E. method

---

1. Initialize parameters  $P_{cross}$ ,  $a$ ,  $N$ ,  $G_{max}$
  2. Initialization of the population
  3. Evaluation of the population in the fitness function
  4. For each particle
    5. Creation of the mutant vector  $v$
    6. Creation of the test solution  $u$
    7. Selection of the best-found solution between  $u$  and  $x_i$
  8. End for
  9. Update the global-best so far
  10. If the maximum number of generations has not been achieved
  11. Go to step 4
  12. Else
  13. End the search
  14. End if-else
- 

## 7. Results

A simulation framework was implemented to validate the performance of the proposed method. The experiment contemplated a variable-voltage energy source that provided the required voltage to the converter. The converter input voltage varied from 28 V to 40 V, which caused the voltage gain to range from 5 to 7.15.

On the other hand, some D.E. algorithm parameters needed to be set, such as the factor  $a$ , the crossover probability  $P_{cross}$ , the number of generations  $G_{max}$ , and the population  $N$  (the number of individuals). This configuration was carried out by observing the performance of the D.E. method for different combinations of values. Since the D.E.'s performance is evaluated considering the achieved input current ripple  $\Delta_{ig}$ , a sensitivity test was implemented to choose the best parameter configuration for reducing the input current ripple. Different combinations of parameter values were set to execute the algorithm for finding the input current ripple. For the crossover probability, we used the values of 0.1, 0.2, and 0.3. The constant factor  $a$  was considered with the values of 1, 10, and 100. The population size included in the test was 20, 30, and 50 individuals. Finally, the maximum number of generations was 100, 200, and 300. After several tests, the parameter combination that best decreased the input current ripple was used in the numerical experiments. These settings are listed in Table 2.

**Table 2.** Parameters of the D.E. method.

Crossover probability $P_{cross}$	0.2
Constant factor $a$	10
Population size $N$	50
Maximum number of generations $G_{max}$	300

Furthermore, the converter of interest involved several parameters that needed to be configured, namely the inductor constant factor, the input voltage, the inductance, and the switching frequency. Table 3 reports the stated parameters, whose values were assigned considering the standard specifications for this kind of converter.

**Table 3.** Parameters of the hybrid switched-capacitor boost converter.

Input voltage $V_g$	28–40 V
Switching frequency $f_s$	50 kHz
Inductor factor $k_L$	0.4
Inductor $L$	200 $\mu$ H

Numerical experiments were carried out to compare the proposed method's performance against the proportional strategy. Only the proportional strategy was considered since it was previously proven that the proportional strategy achieves a lower input current ripple compared to the complementary strategy for a defined operating range; if the proposed strategy provides superior performance compared to the complementary strategy, it can be considered the best strategy.

This test considered several operating points to demonstrate the robustness of the proposed approach. Every operating point represented a different input voltage to the converter, which varied from 28 V to 40 V. Thus, the experiments considered 44 operating points in which the proposed method and the traditional strategy were simulated to obtain 44 input current ripples, one for every operating point.

Furthermore, the values of the parameters described in tables a and b were used in the experiments. Both methods were simulated under the same conditions to guarantee that the comparison was fair. The best-achieved outcomes from the proposed technique, considering 30 independent executions (due to its stochasticity nature), are reported in Table 4. Likewise, the former strategy results are listed in the same Table, where the best input current ripple  $\Delta i_g$  attained between both techniques is emphasized in boldface.

**Table 4.** Optimal parameter values and the input current ripple obtained from the numerical experiments considering the former strategy and the proposed method.

Former Strategy				Proposed Method		
$G$	$D$	$k_d$	$\Delta i_g$	$D$	$k_d$	$\Delta i_g$
5.00	0.7218	0.4000	0.0526	0.7215	0.4054	<b>0.0502</b>
5.05	0.7254	0.4000	0.0770	0.7246	0.4079	<b>0.0715</b>
5.10	0.7289	0.4000	0.1003	0.7279	0.4111	<b>0.0937</b>
5.15	0.7323	0.4000	0.1224	0.7313	0.4134	<b>0.1154</b>
5.20	0.7357	0.4000	0.1441	0.7341	0.4162	<b>0.1336</b>
5.25	0.7389	0.4000	0.1641	0.7373	0.4186	<b>0.1533</b>
5.30	0.7421	0.4000	0.1837	0.7404	0.4194	<b>0.1722</b>
5.35	0.7452	0.4000	0.2022	0.7431	0.4230	<b>0.1882</b>
5.40	0.7483	0.4000	0.2205	0.7460	0.4252	<b>0.2056</b>
5.45	0.7513	0.4000	0.2377	0.7488	0.4268	<b>0.2219</b>
5.50	0.7542	0.4000	0.2540	0.7514	0.4298	<b>0.2369</b>
5.55	0.757	0.4000	0.2694	0.7544	0.4295	<b>0.2527</b>
5.60	0.7598	0.4000	0.2845	0.7569	0.4334	<b>0.2665</b>
5.65	0.7625	0.4000	0.2987	0.7597	0.4359	<b>0.2816</b>
5.70	0.7652	0.4000	0.3126	0.7622	0.4356	<b>0.2944</b>
5.75	0.7678	0.4000	0.3257	0.7646	0.4378	<b>0.3063</b>
5.80	0.7704	0.4000	0.3386	0.7669	0.4411	<b>0.3174</b>
5.85	0.7729	0.4000	0.3507	0.7694	0.4424	<b>0.3299</b>
5.90	0.7753	0.4000	0.3619	0.7720	0.4435	<b>0.3421</b>
5.95	0.7777	0.4000	0.3730	0.7742	0.4463	<b>0.3523</b>

Table 4. Cont.

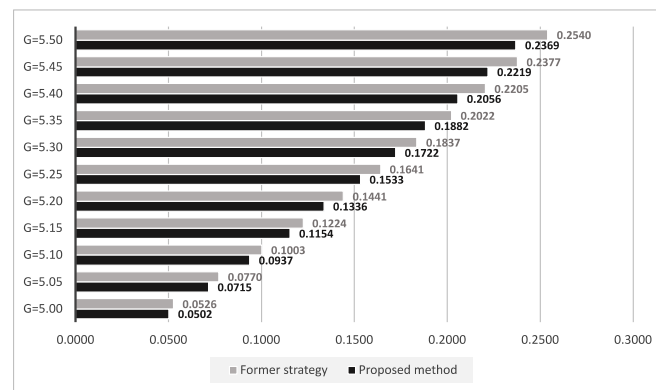
<i>G</i>	Former Strategy			Proposed Method		
	<i>D</i>	<i>k<sub>d</sub></i>	$\Delta i_g$	<i>D</i>	<i>k<sub>d</sub></i>	$\Delta i_g$
6.00	0.7801	0.4000	0.3839	0.7764	0.4470	<b>0.3626</b>
6.05	0.7823	0.4000	0.3935	0.7785	0.4491	<b>0.3713</b>
6.10	0.7846	0.4000	0.4034	0.7807	0.4506	<b>0.3809</b>
6.15	0.7868	0.4000	0.4127	0.7828	0.4517	<b>0.3898</b>
6.20	0.789	0.4000	0.4218	0.7852	0.4537	<b>0.4001</b>
6.25	0.7911	0.4000	0.4302	0.7869	0.4554	<b>0.4067</b>
6.30	0.7932	0.4000	0.4384	0.7890	0.4555	<b>0.4152</b>
6.35	0.7952	0.4000	0.4460	0.7910	0.4571	<b>0.4229</b>
6.40	0.7972	0.4000	0.4534	0.7930	0.4579	<b>0.4303</b>
6.45	0.7992	0.4000	0.4608	0.7948	0.4608	<b>0.4372</b>
6.50	0.8011	0.4000	0.4675	0.7971	0.4589	<b>0.4459</b>
6.55	0.803	0.4000	0.4740	0.7986	0.4625	<b>0.4504</b>
6.60	0.8049	0.4000	0.4805	0.8004	0.4646	<b>0.4569</b>
6.65	0.8067	0.4000	0.4864	0.8022	0.4648	<b>0.4629</b>
6.70	0.8085	0.4000	0.4922	0.8043	0.4641	<b>0.4703</b>
6.75	0.8103	0.4000	0.4979	0.8057	0.4678	<b>0.4739</b>
6.80	0.812	0.4000	0.5029	0.8076	0.4667	<b>0.4803</b>
6.85	0.8137	0.4000	0.5080	0.8094	0.4689	<b>0.4859</b>
6.90	0.8154	0.4000	0.5129	0.8111	0.4678	<b>0.4911</b>
6.95	0.817	0.4000	0.5173	0.8124	0.4722	<b>0.4943</b>
7.00	0.8186	0.4000	0.5216	0.8140	0.4726	<b>0.4988</b>
7.05	0.8202	0.4000	0.5258	0.8157	0.4719	<b>0.5034</b>
7.10	0.8218	0.4000	0.5300	0.8172	0.4751	<b>0.5073</b>
7.15	0.8233	0.4000	0.5336	0.8189	0.4758	<b>0.5122</b>

In Table 4, the best parameter combination values (*D*, *k<sub>d</sub>*) obtained from both strategies are reported. Additionally, it shows the obtained input current ripple  $\Delta i_g$  using those values for every voltage gain *G*. From the Table, a close inspection demonstrates that the lowest input current ripple was reached by the proposed approach for all the experiments. These results are a consequence of the proposed optimization method's search process, which was able to find the optimal values for the duty cycles in such a way that these values led to a decrease in the input current ripple without a change in the required voltage gain.

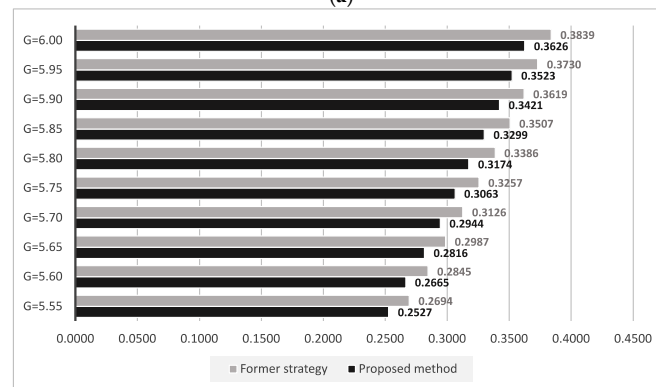
The comparison between the proposed method and the former strategy, in terms of the input current ripple obtained from the numerical experiments, is reported in Figure 7.

Figure 7a–d can be visually analyzed to observe the extent to which the proposed method outperformed the former strategy. For every voltage gain from 5 V to 7.15 V, the statistics show the obtained input current ripple considering both approaches, revealing that the proposed technique found the best parameter combination to further reduce the input current ripple.

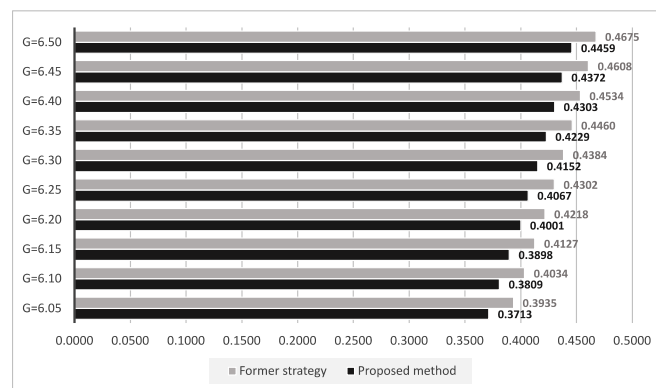
In summary, the proposed method proved its efficiency in finding the best parameter combination to decrease the input current ripple and maintain the required voltage gain. The experimental results support the proposed strategy, in which a different mathematical model that considers independent duty cycles, and the implementation of the D.E. method to optimize the parameter values, achieved better results than the traditional strategy without modifying the converter at a hardware level, instead only making software modifications.



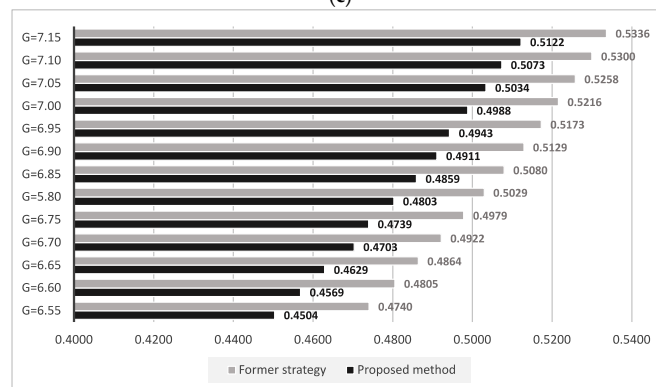
(a)



(b)



(c)



(d)

**Figure 7.** Input current ripple obtained from the former strategy and the proposed method: (a) for voltage gain from 5.00 V to 5.50 V; (b) for voltage gain from 5.55 V to 6.00 V; (c) for voltage gain from 6.05 V to 6.50 V; and (d) for voltage gain from 6.65 V to 7.15 V.

## 8. Conclusions

A novel strategy for reducing the input current ripple of the hybrid switched-capacitor boost converter is proposed in this article. This work aims to optimize the duty cycles of the converter by generating a new model that considers independent duty cycles. However, finding the optimal values for duty cycles when they are independent is not an easy task. Therefore, the proposed strategy includes the implementation of the Differential Evolution algorithm to find the best value combination for the switching pattern to reach high quality at the input current side while satisfying the required voltage gain.

The main objective of the proposed method is to improve the traditional strategy used to reduce the input current ripple. This former strategy considers dependent duty cycles, limiting the possibility of further decreasing the input current ripple and increasing the input current's quality. Furthermore, the proposed approach does not make any changes to the converter at a hardware level. Instead, it only makes software changes.

The proposed method's performance and the former strategy were compared under several experiments, which considered different input voltage values to the converter. The experiments demonstrate that the proposed technique outperforms the former strategy by obtaining a lower input current ripple for all operating points without affecting the required voltage gain.

In future work, an enhanced version of the D.E. algorithm or a different, more recent algorithm can be included. In addition, several swarm-based algorithms can be implemented in order to compare their performances and analyze which could be the best option for finding the optimal duty cycle values. The analysis can be from the perspective of the swarm-based methods and their effectiveness when applied to this kind of constrained optimization problem. Furthermore, if new PWM strategies are reported for the converter under study, a comparison against this strategy can be performed.

**Author Contributions:** J.C.R.-C. and P.M.G.-V. contributed to the conceptualization of the article, from the power electronics point of view; F.B.-C., E.C. and A.M. contributed to the methodology; E.C., A.R. and A.A.-R. contributed to the software, validation, and formal analysis; P.M.G.-V., A.R. and J.C.R.-C. wrote the draft and prepared the manuscript. All authors have read and agreed to the published version of the manuscript.

**Funding:** J.C.R.-C. would like to thank Universidad Panamericana, for their support through the program "Fomento a la Investigación UP 2021" and the project "Estrategias de reducción de variaciones por conmutación y energía almacenada, y optimización en el diseño de convertidores de energía eléctrica", grant number: UP-CI-2021-GDL-01-ING.

**Institutional Review Board Statement:** Not applicable.

**Informed Consent Statement:** Not applicable.

**Data Availability Statement:** Not applicable.

**Acknowledgments:** The authors would like to thank Universidad Panamericana, Tecnológico Nacional de México (Instituto Tecnológico de Ciudad Madero), Universidad de Guadalajara, and Universidad Autónoma Metropolitana.

**Conflicts of Interest:** The authors declare no conflict of interest.

## References

1. Arias, M.B.; Bae, S. Design Models for Power Flow Management of a Grid-Connected Solar Photovoltaic System with Energy Storage System. *Energies* **2020**, *13*, 2137. [[CrossRef](#)]
2. Hou, D.; Lee, F.C.; Li, Q. Very High Frequency IVR for Small Portable Electronics with High-Current Multiphase 3-D Integrated Magnetics. *IEEE Trans. Power Electron.* **2017**, *32*, 8705–8717. [[CrossRef](#)]
3. Ahsanuzzaman, S.M.; Prodić, A.; Johns, D.A. An Integrated High-Density Power Management Solution for Portable Applications Based on a Multioutput Switched-Capacitor Circuit. *IEEE Trans. Power Electron.* **2016**, *31*, 4305–4323. [[CrossRef](#)]
4. Kurdkandi, N.V.; Nouri, T. Analysis of an efficient interleaved ultra-large gain DC–DC converter for DC microgrid applications. *IET Power Electron.* **2020**, *13*, 2008–2018. [[CrossRef](#)]

5. Liu, T.; Yang, X.; Chen, W.; Xuan, Y.; Li, Y.; Huang, L.; Hao, X. High-Efficiency Control Strategy for 10-kV/1-MW Solid-State Transformer in PV Application. *IEEE Trans. Power Electron.* **2020**, *35*, 11770–11782. [[CrossRef](#)]
6. Youn, H.S.; Yun, D.H.; Lee, W.S.; Lee, I.O. Study on Boost Converters with High Power-Density for Hydrogen-Fuel-Cell Hybrid Railway System. *Electronics* **2020**, *9*, 771. [[CrossRef](#)]
7. Balog, R.S.; Krein, P.T. Coupled-Inductor Filter: A Basic Filter Building Block. *IEEE Trans. Power Electron.* **2013**, *28*, 537–546. [[CrossRef](#)]
8. Nag, S.S.; Mishra, S.; Joshi, A. A Passive Filter Building Block for Input or Output Current Ripple Cancellation in a Power Converter. *IEEE J. Emerg. Sel. Top. Power Electron.* **2016**, *4*, 564–575. [[CrossRef](#)]
9. Cheng, M.; Pan, C.; Teng, J.; Luan, S. An Input Current Ripple-Free Flyback-Type Converter with Passive Pulsating Ripple Canceling Circuit. *IEEE Trans. Ind. Appl.* **2017**, *53*, 1210–1218. [[CrossRef](#)]
10. Kim, S.; Do, H. Soft-Switching Step-Up Converter with Ripple-Free Output Current. *IEEE Trans. Power Electron.* **2016**, *31*, 5618–5624. [[CrossRef](#)]
11. Al-Saffar, M.A.; Ismail, E.H. A high voltage ratio and low stress DC-DC converter with reduced input current ripple for fuel cell source. *Renew. Energy* **2015**, *82*, 35–43. [[CrossRef](#)]
12. Rosas-Caro, J.C.; Mancilla-David, F.; Mayo-Maldonado, J.C.; Gonzalez-Lopez, J.M.; Torres-Espinosa, H.L.; Valdez-Resendiz, J.E. A Transformer-less High-Gain Boost Converter with Input Current Ripple Cancellation at a Selectable Duty Cycle. *IEEE Trans. Ind. Electron.* **2013**, *60*, 4492–4499. [[CrossRef](#)]
13. Erickson, R.; Maksimovic, D. *Fundamentals of Power Electronics*, 2nd ed.; Springer: New York, NY, USA; Philadelphia, PA, USA, 2001.
14. Dongyan, Z.; Pietkiewicz, A.; Cuk, S. A three-switch high-voltage converter. *IEEE Trans. Power Electron.* **1999**, *14*, 177–183. [[CrossRef](#)]
15. Wang, C. Investigation on Interleaved Boost Converters and Applications. Ph.D. Thesis, Virginia Polytechnic Institute and State University, Blacksburg, VA, USA, 2009.
16. Soriano-Rangel, C.A.; Rosas-Caro, J.C.; Mancilla-David, F. An Optimized Switching Strategy for a Ripple-Canceling Boost Converter. *IEEE Trans. Ind. Electron.* **2015**, *62*, 4226–4230. [[CrossRef](#)]
17. Wan, W.; Bragin, M.A.; Yan, B.; Qin, Y.; Philhower, J.; Zhang, P.; Luh, P.B. Distributed and Asynchronous Active Fault Management for Networked Microgrids. *IEEE Trans. Power Syst.* **2020**, *35*, 3857–3868. [[CrossRef](#)]
18. Ekinci, S.; Hekimoğlu, B.; Demirören, A.; Kaya, S. Harris Hawks Optimization Approach for Tuning of FOPID Controller in DC-DC Buck Converter. In Proceedings of the 2019 International Artificial Intelligence and Data Processing Symposium (IDAP), Malatya, Turkey, 21–22 September 2019; pp. 1–9.
19. Ekinci, S.; Hekimoğlu, B.; Eker, E.; Sevim, D. Hybrid Firefly and Particle Swarm Optimization Algorithm for PID Controller Design of Buck Converter. In Proceedings of the 2019 3rd International Symposium on Multidisciplinary Studies and Innovative Technologies (ISMSIT), Ankara, Turkey, 11–13 October 2019; pp. 1–6.
20. Hekimoğlu, B.; Ekinci, S. Optimally Designed PID Controller for a DC-DC Buck Converter via a Hybrid Whale Optimization Algorithm with Simulated Annealing. *Electrica* **2020**, *8*, 19–27. [[CrossRef](#)]
21. Izci, D.; Ekinci, S.; Hekimoğlu, B. A novel modified Lévy flight distribution algorithm to tune proportional, integral, derivative and acceleration controller on buck converter system. *Trans. Inst. Meas. Control* **2021**, *8*, 014233122110365. [[CrossRef](#)]
22. Izci, D.; Hekimoğlu, B.; Ekinci, S. A new artificial ecosystem-based optimization integrated with Nelder-Mead method for PID controller design of buck converter. *Alex. Eng. J.* **2021**, *8*. [[CrossRef](#)]
23. Walker, G.R.; Sernia, P.C. Cascaded DC-DC converter connection of photovoltaic modules. *IEEE Trans. Power Electron.* **2004**, *19*, 1130–1139. [[CrossRef](#)]
24. García-Vite, P.M.; del Rosario Rivera-Espinosa, M.; Alejandro-López, A.; Castillo-Gutiérrez, R.; González-Rodríguez, A.; Hernández-Angel, F. Analysis and implementation of a step-up power converter with input current ripple cancelation. *Int. J. Circuit Theory Appl.* **2018**, *47*, 1338–1357. [[CrossRef](#)]
25. Karthikeyan, M.; Elavarasu, R.; Ramesh, P.; Bharatiraja, C.; Sanjeevikumar, P.; Mihet-Popa, L.; Mitolo, M. A Hybridization of Cuk and Boost Converter Using Single Switch with Higher Voltage Gain Compatibility. *Energies* **2020**, *13*, 2312. [[CrossRef](#)]
26. Ogata, K. *Modern Control Engineering*; Prentice Hall: Hoboken, NJ, USA, 2010.
27. Storn, R.; Price, K. A Simple and Efficient Heuristic for global Optimization over Continuous Spaces. *J. Glob. Optim.* **1997**, *11*, 341–359. [[CrossRef](#)]
28. Simon, D. *Evolutionary Optimization Algorithms*; Wiley: Hoboken, NJ, USA, 2013.
29. Erik, C.; Rodriguez, A. *Metaheuristic Computation with MATLAB*, 1st ed.; Taylor & Francis: Boca Raton, FL, USA, 2020.
30. Das, S.; Suganthan, P.N. Differential Evolution: A Survey of the State-of-the-Art. *IEEE Trans. Evol. Comput.* **2011**, *15*, 4–31. [[CrossRef](#)]
31. Pant, M.; Zaheer, H.; Garcia-Hernandez, L.; Abraham, A. Differential Evolution: A review of more than two decades of research. *Eng. Appl. Artif. Intell.* **2020**, *90*, 103479.